Investigation of Halide Ion Release Tunnels of Haloalcohol Dehalogenase from Agrobacterium Radiobacter AD1; Computational Study

Aweke Mulu Belachew[1,3(✉)] and Tang Laxia[1,2]

[1] School of Life Science and Technology, University of Electronic Science and Technology of China, Chengdu 610054, China
aweke.mulu@aastu.edu.et
[2] Centers for Informational Biology, University of Electronic Science and Technology of China, Chengdu 610054, China
[3] College of Applied Science, Addis Ababa Science and Technology University, P.O.BOX 16417 Addis Ababa, Ethiopia

Abstract. The Halohydrine dehalogenase (HheC), active site is buried deep inside the structure of the enzyme and to enter the active site, the substrate must cross via the body of the enzyme called tunnels. In several studies revealed that they have been influenced substrate selectivity, stability and activity of enzymes. Know a day, identifying and understanding how tunnels exert selectivity, stability, and activity regulation of enzymes have been growing interest in the fields of computational approach and enzyme engineering. As far as, the HheC concerned studies suggest that the release of chloride ion determines the overall activity of the enzyme and thus tunnels are assumed to exist. Swiss-Modell, Auto dock 3.2, Gromacs 5.2.1, Caver 3.0, and RAMD computational techniques were applied to identify and analyze tunnels and how chloride ions migrate through these tunnels. The purpose of this study is to identify tunnels and analyzes how to influence Chloride ion-releasing activity in the HheC enzyme and provide prerequisite data for wet-lab experiment used to improve overall activity. In this study, we found the presence of Chloride ion narrowed tunnels compare to free HheC enzyme. Moreover, conformation difference, tunnel lining residues and bottle-neck residues were identified for next wet-lab experiment. Future wet-lab investigations to validate the role of residues that are found in tunnel lining could be needed to engineer the activity of HheC.

Keywords: Halide ion release tunnels · Halohydrine dehalogenase · Caver · Molecular dynamic simulation

1 Introduction

Recent experimental developments have revealed the biocatalytic properties of Halohydrine dehalogenase (HHDHs) toward both aromatic and aliphatic Halohydrine to yield Hydrogen, chloride and epichlorohydrine [1, 2]. The field has gradually broadened to computational study as the crystal structure of enzymes purified and determined. The

M. L. Berihun (Ed.): ICAST 2021, LNICST 412, pp. 365–376, 2022.
https://doi.org/10.1007/978-3-030-93712-6_25

Halohydrine dehalogenase (HheC) from the bacterial species Agrobacterium radiobacter strain AD1 has always been under constant investigation [1–3]. This enzyme has homo tetramer domain and each monomer with seven beta strand and extended C-terminus [3]. In the past two decades, the stretch of the C-terminal amino acids, halide binding site amino acids, and active site entrance amino acids have played a significant role in HheC engineering research [2, 4, 5]. This field closely follows the pattern of improving HheC enzyme activity, selectivity and stability by engineering aforementioned sites. However, the active site is buried inside the structure of the HheC, and substrates, as well as products, pass through the body of the enzyme through a tunnel [2]. Moreover, a study has shown that tunnels differentiation among substrates, synchronization of the order of catalytic steps, and reactions that require the number of substrates [14]. Chloride ion releasing tunnel has been shown significant impact on the activity, stability, and selectivity of the HheC tunnel [1, 2, 4, 5]. The available data is limited and no previous study has focused on number and chloride ion egress tunnels and egress kinetics study of HheC enzyme. An approach similar to ours has been presented before in [6] showed that a halide releasing tunnel conformational change preceding the release of halide ion from the active site structure of HheC. Despite the success of this work [6] in certain aspects, it still suffers from short simulation time to produce ensemble structures for tunnel computation. Some other prior work has examined this issue but, the focus was more on the conformational change that occurs in the loop region and lead solvation of the active site that facilitates halide ion escape from haloalkane dehalogenase [4, 5]. This method extends prior work by its unique consideration of the chloride ion release pathway, identification of tunnel lining residues for engineering the accessibility of tunnels and conformational change of HheC tunnels. In general work in this area is in its infancy and is somewhat limited to tunnel selectivity for entry/release of a specific substrates and products.

Until now, tunnels have been studied by using X-ray crystallography, steady-state kinetics, pre-steady-state kinetics, and molecular modeling approach [30, 31]. However, tunnels shape and physicochemical properties regularly change due to influence of thermal, ligand and substrates binding, solvent, and other changes in the surrounding environment [32]. A combination of wet-lab and dry studies is often required to examine the conformational change of enzymes tunnels [31]. Therefore, this extends a dynamic outlook for the enzyme engineers as frequently the dynamics of the enzyme active site are limited to optimize the reactive substrate binding. Recent theoretical developments have revealed that, there are a number of methods that can be used to investigate product releasing tunnel pathway. A number of works have been reported by using Random Acceleration Molecular Dynamics, Steered Molecular Dynamics, Metadynamics and Dynamic Map Ensemble Approaches [5–11]. In other word, dry experiments could form a close relation with wet experiment. In this work, we characterize different aspects of tunnels by using a CAVER 3.0, Gromacs and RAMD simulation in both free enzyme and chloride ion-enzyme complex. This strategy is common in proteins tunnel computation studies. For instance, it has computed tunnels in β2-adrenergic receptor, human cytochrome P450 enzymes, haloalkane dehalogenase and liver fatty acid binding protein [8–11]. As far as we know, no preceding study has investigated halide releasing tunnels. However, this issue has been considered by recent work [6] with a very short simulation time, which is unreasonable. Moreover, few

studies have focused on indirect study on tunnel activity. To overcome the shortcomings of previous studies outlined above, we propose molecular dynamic simulation for 100 ns. In this work we look to improve our earlier approach in two key areas, the RAMD simulation of novel chloride releasing tunnels and key structural changes that take place during chloride dissociation. In analogy with other procedures, this approach has the advantage of giving us an idea to render novel mechanistic insights into HheC tunnel wet-lab engineering. After rigorous examination, it was discovered that tunnels structure and flexibility difference between halide-enzyme complex and free enzyme based on root-mean-square fluctuation (RMSF), root mean-square deviation (RMSD) and evolution of secondary structures with time. Further investigation can be undertaken to explore tunnel lining residues and bottleneck residues. There are some major modifications planned in the future development of experimental study.

2 Results and Discussion

This study incorporates molecular dynamics (MD) simulation, Caver 3.0 and random accelerate molecular dynamics (RAMD) simulation techniques to investigate the chloride ion releasing tunnels in 100 ns simulated HheC chloride ion complex and free HheC enzymes. This technique utilizes a structures consist of free-HheC enzyme and HheC-chloride ion complex, which stabilized by isothermal-isobaric NPT and NVT ensembles based classical MD simulation for 1000 ps (Sup Fig. 1). Next, we evaluated the residue RMSD to analyze the residue behavior of both free-HheC enzyme and HheC-chloride ion complex during 100 ns simulations. In the literatures, RMSD has been extensively investigated to measures protein flexibility, effect of bound substrate and product to control active site accessibility as well as, the average distance between backbone atoms [22, 23].

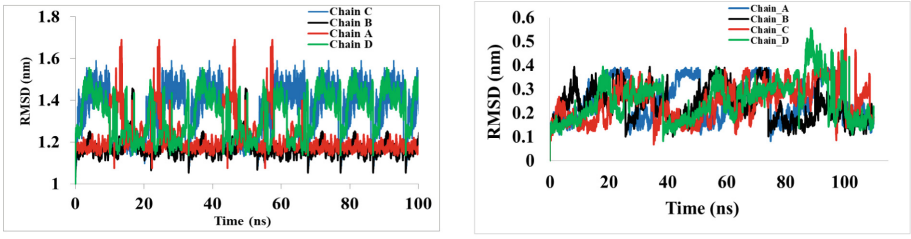

Fig. 1. The root-mean-square deviation (RMSD) value for A) Free HheC-enzyme, and B) HheC-Chloride ion complex analysis chain A (Blue), Chain B (black), Chain C (red) and Chain D (green) (Color figure online)

According to the result of the RMSD plot, all free HheC chains showed equilibration throughout the simulation, and chain D revealed high flexibility between 10–20 ns, 20–30 ns, 40–50 ns, and 58–60 ns (Fig. 1). In HheC-Chloride ion complex types, conformational flexibility reduced and destabilized by the binding of chloride

ion compare to free HheC enzyme, as revealed from the RMSD calculation (Fig. 2). Other groups confirmed that binding of ligand to HheC enzyme decreased and destabilized backbone flexibility, which is consistence with this study [2, 23, 24]. The RMSD presented here, used to test for conformations characteristics and confirm which of the regions of high mobility adequately illustrate the differences on the conformational sampling between free-HheC and HheC-Chloride Ion Complex over 100 ns. In the course of the last 100 ns simulations, the RMSD values for HheC-Chloride ion complex chains decrease with average values from 0.1 nm to 0.4 nm and remain unstable throughout simulation time. Here, free HheC enzyme back bone displayed mean RMSD estimations between 1.1 Å and 1.5 Å. In comprehensive, a higher backbone RMSD value indicated greater movement; conversely, lower residue RMSD value indicates lower movement. Evidence from several MD studies indicated that RMSD used to understand enzymatic mechanisms and to investigate selective unbinds [25, 30].

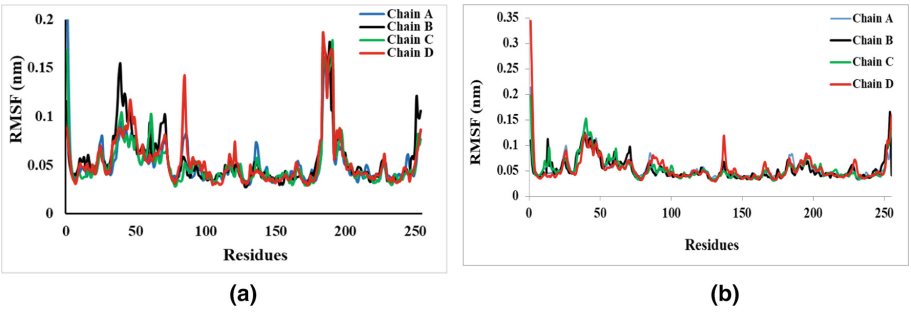

Fig. 2. RMSF results for backbone atoms of A) free-HheC enzyme and HheC-Chloride ion complex chain A (Blue), Chain B (black), Chain C (green) and Chain D (red), which are plotted along with the residues (gray bars). (Color figure online)

Here, we proposed to predict whether the chloride ion disturbs the dynamic behavior of HheC residues, which are important to investigate the role of bottle-neck residues and tunnel-lining residues in chloride ion releasing mechanism. The RMSF values of HheC-chloride ion complex and free-HheC enzyme structures were obtained and shown in Fig. 4. Interpretation of fluctuation score described that the higher degree of flexibility observed in free-HheC enzyme structures between residues 80–100, 150–189, and 200–248 than HheC-chloride ion complex structures (Fig. 2a). The root-mean-square-fluctuation (RMSF) of the backbone revealed comparable motion in the inside of free-HheC and HheC-chloride ion complex (Fig. 2b). As seen in the figure, aforementioned residues of HheC-chloride ion complex produced the clear changes, which mainly concentrate the region between 80–100, 150–189, C-terminus and 200–248 and a portion of 250 residues, surrounding the exit of the chloride ion tunnels (Fig. 4b). In this position the free HheC enzyme showed higher flexibility. Several landmark studies, observed the loop secondary structures tend to fluctuate more than others molecular moieties [25, 30].

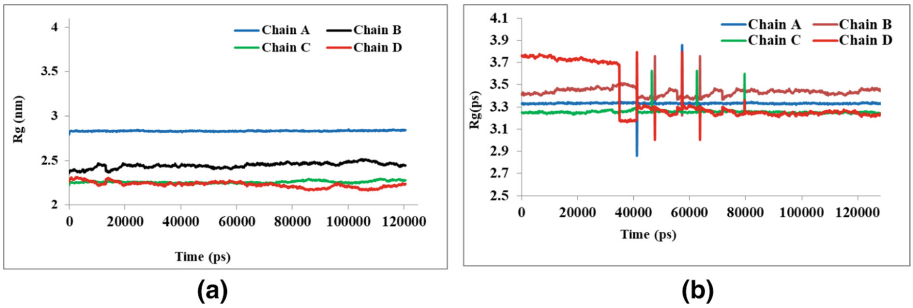

Fig. 3. Time evolution of the radius of gyration (Rg) values for A) HheC-Chloride ion complex B) free-enzyme analysis chain A (Blue), Chain B (black), Chain C (green) and Chain D (red), which are plotted along with the time (gray bars) (Color figure online)

The radius of gyration plot for the backbone of HheC enzyme models versus time at 300 K is shown in Fig. 3. To observe the outcome of the chloride ion on HheC enzyme packing, the radius of gyration (Rg) was calculated. The higher Rg values indicate loose packing of HheC structure, which means conformation that is more flexible. In this context, significant difference between free-HheC and HheC-chloride ion complex observed according to Rg analysis (Fig. 3). Rg value for free-HheC showed higher value between 3.1–3.5 nm and except, Chain D remain unstable until the end of 4 ns simulation (Fig. 2b). This implies that there is high probability to re-duce compactness of HheC Enzyme between during simulation. Studies have demonstrated the strong and consistent link between small molecule interactions, and their role in conformational rearrangement and dynamics in biocatalysts [30].

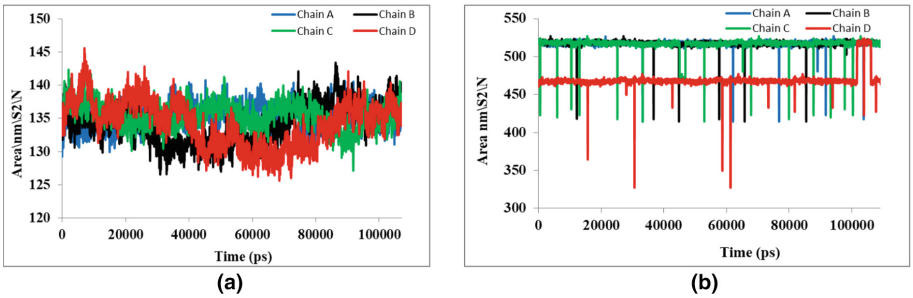

Fig. 4. Solvent accessibility surface area (SASA) analysis for A) the HheC-chloride ion complex and B) free-HheC enzyme structures chain A (Blue), Chain B (black), Chain C (green) and Chain D (red), which are plotted along with the time (gray bars). (Color figure online)

Similarly, solvent dynamics inside the biomolecule solvation layer play vital part in enzyme catalysis, but thoughtful of its role is delayed by its complexity [26, 28, 30]. Here, we studied Solvent accessibility surface area SASA analysis between the HheC-chloride ion complex and free-HheC enzyme structures. Increased value of SASA in

the HheC-chloride ion complex indicates its comparatively not wrinkled nature as compared to the free-HheC enzyme. Change of SASA in HheC-chloride complex and free-HheC enzymes shown in Fig. 4. For all chains in free-HheC enzyme structures showed similar fashion of deviation until 100 ns from the initial structure (Fig. 4a). HheC-chloride ion complex structures showed similar fashion of deviation until 100 ns from the initial structure, but HheC-chloride ion complex structure showed greater value of SASA than free-HheC enzyme structures. The average SASA value was between 450–550 nm in HheC-chloride ion complex (Fig. 4b), whereas the HheC-chloride ion complex structures showed average SASA value of between 130–145 nm, respectively, as depicted in Fig. 4a. Literature review showed that different SASA structures have been seen for Apo-enzyme and Holo-enzyme experimental and computational studies [26, 28, 30]. Inconsistent with other studies the accessibility of active sites is being controlled by chloride ion binding and unbinding. From this stand-point, SASA could be considered tunnels as closed or open and shown the active site isolated from or connected to the bulk solvent.

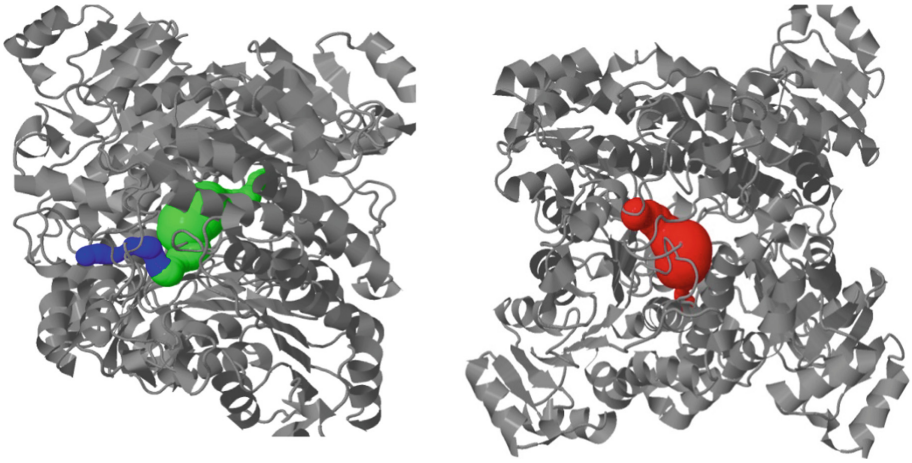

Fig. 5. Comparison of the HheC-chloride ion complex (left) and free HheC (right). The main tunnel is closed by the introduced chloride ion (in blue and green) (Color figure online)

For this investigation, we examined the tunnels assembled from each snapshot using CAVER 3.0.2 [29]. It has been experimentally demonstrated that Ser132, Tyr145 and Arg149 active site residues and we employed as starting point of tunnels computation. Our results demonstrated that there are three significant tunnels i.e. one tunnel from free HheC and two tunnels from HheC-Chloride ion complex, with clustering threshold of the pathway at 4.0 Å (Table 1). Chloride discharging tunnels revealed in Fig. 5. In this investigation, two tunnels identified in HheC chloride ion complex, while one tunnel found in free HheC, with clustering threshold of the pathway at 4.0 Å. In line with previous studies, tunnels width and length used to assess geometric based tunnel identification programs [2]. Therefore, we showed that top four tunnels with

shorter length and wider structure were identified (Table 1). Here we compare the results of the HheC chloride ion complex tunnels with that of the free HheC tunnels. This showed that chloride ion narrowing tunnels. A similar pattern of results obtained in priorities. There aren't distinct tunnels with preferences higher than that shown in Table 1. In the meantime, amino acids lining up tunnels, as well as residues creating bottlenecks tunnels were recognized. Thoroughly, twenty-eight (28) essential residues were revealed in the bottleneck and tunnels by caver 3.0.2. From these results several new important residues such as, 84 P, 137 G, 186 F, 245 M and 248 R, 162 Q, 232 L, 233 T, 162 Q, 247 Q, 177 Y, 187 Y, 191 P, 192 W, 195 E, 197 Q, 198 H, 201 H, 204 K, 205 V, 236 V, 238 W, 243 F, 244 P, 86 F, 138 P, 139 W, 140 K, 141 Q, 142 L, 165 Q, and 160 S found in tunnel-2 and tunnel-3 (Table 1). Our results demonstrated that new important residues that we discovered are located in the bottlenecks and tunnels of both free HheC and HheC-chloride ion complex. These include 131 T, 132 S, 134 T, 130 I, and 133 A. Furthermore, sections close to the individual tunnels revealed the most vital conformational variation inside free HheC (Fig. 2). Conversely, thought of the chloride ion release occasion by classical MD simulation was not satisfactory owing to the very robust electrostatic interactions between chloride ion and tunnel site residues. Therefore, RAMD simulation was desirable. The majority of prior research has applied RAMD to a wide range of proteins tunnel engineering for modifying activity [6, 7, 9]. In the context of this study, after a series of MD simulation and CAVER analysis, RAMD simulation was executed on the fifty various data structures of HheC chloride ion complex, which were extracted from classical MD simulation. Recent theoretical developments have revealed that 0.85 kcal Å−1 mol−1 force applied on chloride ion. In this study, when the random 0.85 kcal Å−1 mol−1 force applied on chloride ion, it destabilized the interactions between the chloride ion and tunnel residues and finally explored a new direction to exit. In line with previous CAVER analysis chloride ion throwing out through two dissimilar tunnels: tunnels B and C (Table 1).

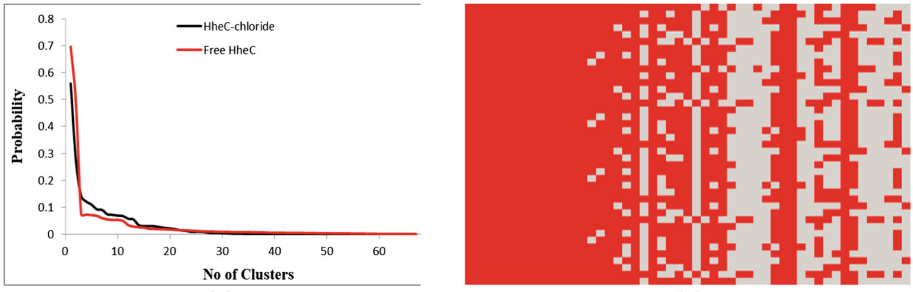

Fig. 6. A) Probabilities of the 67 largest clusters of free HheC-(red) and HheC-Chloride-(black) enzyme, B) Heat map reflecting the time progression of bottleneck radii of private tunnel clusters. Per row corresponds to one cluster of 10000 pictures. The gray color symbolizes that no tunnel from an assigned cluster was recognized in a given picture.(Color figure online)

During tunnel computation, the structure produces dozens of tunnels, which are difficult to determine the steadiness of distinct tunnels over time. Here, we focused on the tunnel that is persisted throughout the simulation and serves as the chloride ion release pathway and for further detailed exploration. For this study tunnels in one static image with a heat map exhibits every distinguished tunnel in the molecular dynamics in Fig. 6b. A rectangle in the heat map corresponds to the bottleneck of a tunnel at a distinct position in time and the intensity encodes the bottleneck size. The paint slider to the right outlines the plotting of bottleneck size to paint. A lower limit of the acceptable bottleneck extent can be interactively quantified on the paint slider. Bottlenecks under this boundary are shown in white. A vertical line in the all tunnel heat agrees to the time-based development of a specific tunnel over time. White rectangles on such a line specify time steps where the tunnel is either closed or it is too small for the examined ligand. A horizontal line corresponds to all the tunnels given at a specific point in time. In this study, tunnel is fixed according to their significance from left to right and at the left of the heat map the most encouraging tunnels are shown. The importance of a given tunnel is calculated by averaging the sum of tunnel throughputs over all pictures. If the tunnel is closed at given picture, zero value is used, which rejects further consideration. And also, transient tunnels are depicted in the right part of the heat map and showed the temporal location of the open part of the tunnel. Generally, this shows graphic variance if the tunnel is open for a continuous serving of time or if the time steps when the tunnel is open are dispersed discontinuously throughout the molecular dynamics and govern if the chloride ion could be followed the tunnel. This is a candidate for further exploration.

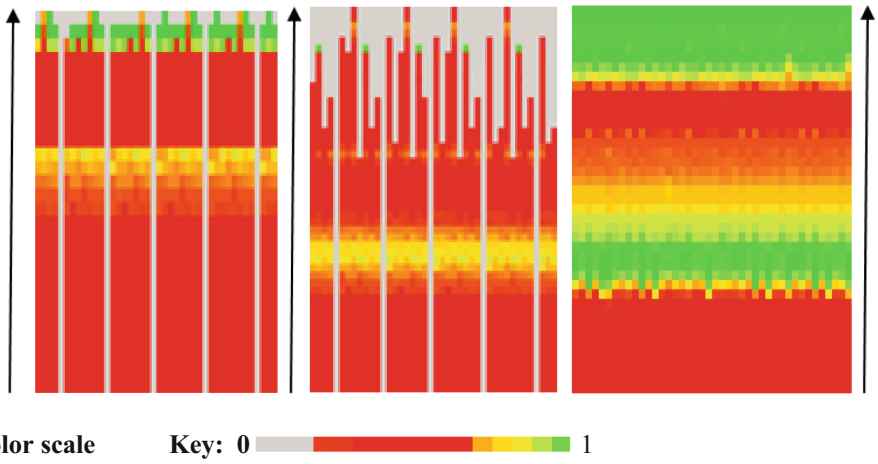

Fig. 7. Heat map visualizing the time evolution of the tunnel profile for 100 ns simulation. The first two columns depict the average profile for the HheC-Chloride complex and the third column outlines free HheC pictures. The color of an element with coordinates x and y signifies the radius of a presented tunnel in 10000 snapshots and 625 distance interval.

After the filtering stage, we explored the top three selected tunnels as shown in Fig. 7 by using bottle-neck. Here, we used different bottleneck sizes and compute with various frames of the bottleneck, which restricts the maximal size of relevant chloride ion outlet. As shown in Fig. 7 We address this problem by including an interactive Single Tunnel Heat Map. In this context, we performed the tunnel analysis several times, with a small bottleneck radius between 0.5–0.9 Å. The Single Tunnel Heat Map representation now displays only one tunnel from free-HheC and two from HheC-chloride ion complex at a time (Fig. 7). The upright axis again signifies the time domain. The horizontal axis now signifies the tunnel length and the color of separate rectangles encrypts the thickness of the tunnel at conforming positions along the tunnel centerline. The grey rectangles depict that the tunnel is closed or the bottle-neck size is below the user-defined threshold. We can use the pre-computed information about the tunnel thickness in the closed parts as well which is fixed as grey value. Darker grey values link to smaller bottle-neck widths of the closed tunnel. Mostly, we get an overview of the tunnel behavior of HheC when changing the minimum bottleneck size, which helps them to discovery an appropriate threshold value. This value then outlines the maximal size of a chloride ion which could be transported via this tunnel. An all Tunnels Heat Map is a much more collected image as compared to the Single Tunnel Heat map. In an All Tunnel Heat map a tunnel is reduced to its bottleneck, whereas in a Single Tunnel Heat map the complete tunnel at an exact idea in time is given. By studying the throughput of tunnels using the all Tunnel Heat map and Single Tunnel Heat map, selected candidate tunnels for the transport of a chloride ion of a specified size to the HheC active site.

Table 1. Features of tunnels in HheC-chloride complex and free-HheC enzymes. Tunnels B, C in HheC-chloride complex and tunnel B in free-HheC, respectively

Tunnels	Bottleneck Radius	Tunnel length	Priority	Tunnels residues	Bottleneck residues
Tunnel-A	1.046 ± 0.05	14.14 ± 0.007	0.60	12 F,83 A,84 P,86 F, 130 I, 131 T,132 S, 133 A, 134 T, 139 W, 142 L, 145 Y, 149 R, 175 P, 176 Q,177 Y, 178 L, 184 P, 185 Y, 186 F, 187 Y, 188 P, 192 W, 249 W, 80 N, 82 F, 85 Q, 174 G	P138, K161,P244, M245, I246, G137, G242, 249W, 186F, 84P, 187 Y,184 P,139 W,185 Y, 86 F, 145 Y
Tunnel-B	0.9 ± 0.003	15.9 ± 0.1	0.56	131 T,132 S,134 T, 135 P, 136 F, 145 Y, 149 R, 150 A, 152 A, 153 C, 154 T, 157 N, 161 K, 235 Q, 236 V, 238 W, 138 P, 130 I, 133 A, 146 T, 147 S, 148 A, 151 G, 174 G, 234 G, 237 F, 137 G and 151 G	132 S, 149 R, 131 T, 135 P,133 A, 153 C,134 T, 150 A,174 G, 146 T, 238 W, 145 Y, 152 A and 148 A
Tunnel-C	0.87 ± 0.001	12.3 ± 0.02	0.499	131 T,132 S, 134 T,135 P, 136 F,145 Y,149 R,150 A, 152 A,153 C,154 T,157 Q, 160 S, 161 K,165 E,235 Q, 236 V, 238 W, 86 F,135 P, 136 F, 138 P, 139 W, 140 K, 141 Q,142 L, 150 A,153 C, 154 T,157 E, 177 Y,187 Y, 191 P, 192 W, 195 E, 197 Q,198 H, 201 H, 204 K,205 V, 236 V, 238 W, 243 F, 244 P, 246 I, 247 Q, 130 I, 133 A, 146 T, 147 S,148 A,151 G, 162 Q, 174 G,232 L,233 T,234 G,237 F,84 P, 137 G, 186 F,245 M, and 248 R	132 S,149 R, 131 T,135 P, 133 A,153 C, 134 T,150 A, 174 G,146 T,238 W,145 Y, 152 A, and 148 A

The enzyme backbone conformation altered during chloride ion detachment, with spin of a few residue side chains further increasing the opening of tunnel A to let release of the chloride ion (Fig. 4a). Tunnel B lies between the 82–87 loop and 95–120 loop being on the reverse side from tunnel A. Certain parts of tunnel B were thought to be flexible, which specified that an open pathway could form at this region (Fig. 4b). Tunnel C is lined mostly by 82–87 loop. In this region, it is not a predominantly easy process to untie the side-chain packing of hydrophobic residues, so C was the tunnel least regularly used for ligand detachment (Fig. 4c). Meanwhile, we recognized key residues controlling the exit and entrance of HheC tunnels as showed in Table 1. Identification of the detachment ways will offer further mechanistic insights into HheC, which will benefit modification of HheC activity.

3 Conclusions

In this study, extensive MD simulations, CAVER 3.0 and RAMD were performed to examine the chloride ion releasing tunnel of HheC. Tunnels that facilitate the release of chloride ion in the free HheC and HheC-chloride complex enzymes were considered, and it was established that binding of chloride ion could meaningfully narrow the tunnels. Moreover, a conformational cluster analysis of the tunnel loop region specified its vital role in narrowing the chloride ion releasing tunnels. And also, amino acids making up tunnels and tunnel bottlenecks were identified. It was found that all three active site residues were located along the tunnel-site loop region, with the majority being situated along the main part of the enzyme. These findings provide a potential explanation for the conformational variation of the tunnel-site loop induced by the binding of chloride ions. Future research should consider the potential effects of engineering residues making up tunnels and tunnel bottlenecks more carefully, and their roles on activity of enzyme further inspect experimentally.

References

1 van Hylckama Vlieg, J., et al.: Halohydrin Dehalogenases are structurally and mechanistically related to Short-Chain Dehydrogenases/Reductases. J. Bacteriol. **183**(17), 5058–5066 (2001)
2 Tang, L., Torres Pazmiño, D., Fraaije, W.M., de Jong, M.R., Dijkstra, B.W., Janssen, D.B.: Improved catalytic properties of Halohydrin Dehalogenase by modification of the Halide-Binding Site. Biochemistry, **44**(17), 6609–6618 (2005)
3 Koopmeiners, J., et al.: HheG, a Halohydrin Dehalogenase with activity on cyclic epoxides. ACS Catal. **7**(10), 6877–6886 (2017)
4 Tang, X.L., Ye, G.Y., Wan, X.Y., Li, H.W., Zheng, R.C., Zheng, Y.G.: Rational design of halohydrin dehalogenase for efficient chiral epichlorohydrin production with high activity and enantioselectivity in aqueous-organic two-phase system. Biochem. Eng. J., **161**, 107708 (2020)
5 Estévez-Gay, M., Iglesias-Fernández, J., Osuna, S.: Conformational landscapes of Halohydrin Dehalogenases and their accessible active site tunnels. Catalysts **10**(12), 1403 (2020)

6 Tao, Y.: Theoretical and computational research on halide ion release channel of Haloalcohol Dehalogenase from Agrobacterium Radiobacter AD1. Unpublished Manuscript (2014)
7 Pan, Q.R., Li, M., Wang, B., Huang, H., Han, W.: Random acceleration and steered molecular dynamics simulations reveal the unbinding tunnels in adenosine deaminase and critical residues in tunnels. RSC Adv. **10**, 43994 (2019)
8 Potterton, A., et al.: Ensemble-based steered molecular dynamics predicts relative residence time of A2A receptor binders. J. Chem. Theory Comput., **15**, 3316−3330 (2019)
9 Vilar, S., Karpiak, J., Berk, B., Costanzi, S.: In silico analysis of the binding of agonists and blockers to the β2-adrenergic receptor. J. Mol. Graph. Model. **29**(6), 809–817 (2011)
10 Akram, M., Waratchareeyakul, W., Haupenthal, J., Hartmann, J.W., Schuster, D.: Pharmacophore modeling and in Silico/in Vitro screening for human cytochrome P450 11B1 and cytochrome P450 11B2 inhibitors. Front. Chem. https://doi.org/10.3389/fchem.2017.00104
11 Daniel, L., Buryska, T., Prokop, Z., Damborsky, J., Brezovsky, J.: Mechanism-based discovery of novel substrates of Haloalkane Dehalogenases using in silico screening. J. Chem. Inf. Model **55**(1), 54–62 (2015)
12 Mujwar, S., Kumar, V.: Computational drug repurposing approach to identify potential fatty acid-binding Protein-4 inhibitors to develop novel antiobesity therapy. Assay Drug Dev. Technol. **18**(7), 1–20 (2020)
13 Gordon, J.C., Myers, J.B., Folta, T., Shoja, V., Heath, L.S., Onufriev, A.: H++: a server for estimating pKas and adding missing hydrogens to macromolecules, Nucleic Acids Res. **33**, W368–71 (2005)
14 Laskowski, R.A., MacArthur, M.W., Thornton, J.M.: PROCHECK: validation of protein structure coordinates, in International Tables of Crystallography, Volume F. In: Rossmann, M.G., Arnold, E. (eds.) Crystallography of Biological Macromolecules, pp. 722–725. Dordrecht, Kluwer Academic Publishers, Netherlands (2001)
15 Hess, B., Kutzner, C., van der Spoel, D., Lindahl, E.: GROMACS 4: algorithms for highly efficient, Load-Balanced, and scalable molecular simulation. J. Chem. Theory Comput. **4**(3), 435–447 (2008)
16 MacKerell, A.D., et al.: J. Phys. Chem. B. **102**, 3586–3616 (1998)
17 Wang, J., Wolf, R.M., Caldwell, J.W., Kollman, P.A., Case, D.A.: Development and testing of a General Amber Force Field. J. Comput. Chem. **25**(9), 1157–1174 (2004)
18 Jorgensen, W.L., Chandrasekhar, J., Madura, J.D., Impey, R.W., Klein, M.L.: Comparison of simple potential functions for simulating liquid water. J. Chem. Phys. **79**, 926 (1983)
19 Vardeman, F.C., Stocker, M.K., Gezelter, J.D.: The Langevin Hull: constant pressure and temperature dynamics for non-periodic systems. J. Chem. Theory Comput., **7**(4), 834–842 (2012)
20 Humphrey, W., Dalke, A., Schulten, K.: VMD: visual molecular dynamics. J. Mol. Graph. **14**(1), 33–38 (1996)
21 Schrodinger, L.L.C.: Book the PyMOL Molecular Graphics System, Version 1.3r1. The PyMOL Molecular Graphics System, Version 1.3r1 (2010)
22 Sargsyan, K., Grauffel, C., Lim, C.: How molecular size impacts RMSD applications in molecular dynamics simulations. J. Chem. Theory Comput. **13**(4), 1518–1524 (2017)
23 dos Santos, G.E., Fariab, X.R., Rodrigues, R.C., Bello, L.M.: Molecular dynamic simulations of full-length human purinergic receptor subtype P2X7 bonded to potent inhibitors. European J. Pharm. Sci. **152**, 105454 (2020)
24 Cui, Y.L., et al.: Structural and dynamic basis of human cytochrome P450 7B1: a survey of substrate selectivity and major active site access channels. Chem. European J. **19**(2), 549–557 (2013)

25 Mortier, J., Rakers, C., Bermudez, M., Murgueitio, M.S., Riniker, S., Wolber, G.: The impact of molecular dynamics on drug design applications for the characterization of ligand–macromolecule complexes. Drug Discovery, **20**(6), 1–17 (2015)
26 Verma, R., Mitchell-Koch, K.: In silico studies of small molecule interactions with enzymes reveal aspects of catalytic function. Catalysts **7**(7), 212 (2017)
27 Du, X., et al.: Insights into protein–ligand interactions: mechanisms, models, and methods. Int. J. Mol. Sci. **17**(2), 144 (2016)
28 Schwartz, S.D., Schramm, V.L.: Enzymatic transition states and dynamic motion in barrier crossing. Nat. Chem. Biol. **5**, 551–558 (2009)
29 Marques, S.M., Bednar, D., Damborsky, J.: Computational study of protein-ligand unbinding for enzyme engineering. Front. Chem. **6**(650), 1845–1852 (2018)
30 Prokop, Z., Gora, A., Brezovsky, J., Chaloupkova, R., Stepankova, V., Damborsky, J.: Engineering of protein tunnels: keyhole-lock-key model for catalysis by the enzymes with buried active sites. In: Protein Engineering Handbook, vol. 3, pp. 421–464. WileyVCH, Weinheim (2012)
31 Chovancova, E., et al.: CAVER 3.0: a tool for the analysis of transport pathways in dynamic protein structures. PLoS Comput. Biol., **8**(10), e1002708 (2012)
32 Pierce, L., Ferrer, R.S., McCammon, A., de Oliveira F.A., Walker, C.R.: Routine access to millisecond time scale events with accelerated molecular dynamics. J. Chem. Theory Comput., **8**(9), 2997-3002 (2012)
33 de Jong, R.M., et al.: Structure and mechanism of a bacterial haloalcohol dehalogenase: a new variation of the short-chain dehydrogenase/reductase fold without an NAD (P) H binding site. EMBO J. **22**, 4933-4944 (2003)
34 de Jong, R.M., Tiesinga, J.W.J., Villa, A., Tang, L., Janssen, B.D., Dijkstra, W.B.: Structural basis for the Enantioselectivity of an Epoxide Ring Opening Reaction Catalyzed by Halo Alcohol Dehalogenase HheC. J. Am. Chem. Soc., **127**(38), 13338–13343 (2005)
35 Cook, I., Wang, T., Almo, C.S., Kim, J., Falany, N.C., Leyh, S.T.: The gate that governs sulfotransferase selectivity. Am. Chem. Soc., **52**(2), 415–424 (2013)
36 Bottaro, S., Lindorff-Larsen, K.: Biophysical experiments and biomolecular simulations: a perfect match? Science **361**, 355–360 (2018)